



Simultaneous synthesis of nanoporous zinc oxide and carbon dots via biopolymer dual templating

Kanako Kimura^{a,b}, Simran Channa^{a,c}, Georgia McCluskey^c, Alexander Kulak^c, Yi-Yeoun Kim^c, Natalia N. Sergeeva^{a,b,*}

^a School of Design, University of Leeds, Leeds LS2 9JT, UK

^b The Leeds Institute of Textiles and Colour, University of Leeds, Leeds LS2 9JT, UK

^c School of Chemistry, University of Leeds, Woodhouse Lane, Leeds LS2 9JT, UK

ARTICLE INFO

Keywords:

Polysaccharides
Nanoporous zinc oxide
Hydrothermal synthesis
Carbon nanoparticles
Antioxidant activity

ABSTRACT

Dual templating is an effective strategy to create multiple inorganic functional materials with enhanced structural, optical, and biological properties. We demonstrate how biopolymer directly dictates the internal structure of zinc oxide. Here, a thermally degradable biopolymer, chitosan, is used as a structural template to produce internal nano pores of zinc oxide, while biopolymer transforms into highly luminescent carbon dots in the same solution. It is thought that zinc oxide is nucleated within the polymer network and continues to grow by engulfing the network into its crystalline structure. This is followed by thermal degradation of polymer template and its carbonisation into carbon dots. The synthesised porous zinc oxide-chitosan composites are characterised by PXRD, FT-IR, TGA, and SEM. The shape and size of pores created within zinc oxide crystals are assessed by FIB-SEM analysis. Finally, the antioxidant activity of the synthesised composites is significantly enhanced even at low concentrations from 20% in pure zinc-oxide to 100% in the synthesised composites.

1. Introduction

Biotemplating using biopolymers is an attractive biomimetic strategy to create novel materials through effective control over the final structure by directing, positioning, and linking multiple components during synthesis [1]. A real advantage of these macromolecules is their structural specificity such as well-defined monomeric sequence, stereochemistry, and specific chain length. Among available biotemplates, polysaccharides are abundant sustainable alternatives that can be employed to assist in synthesis of inorganic materials by providing a well-defined matrix for growth. This polymeric network can be later removed by mineralisation, calcination or sintering creating nano-materials with long-range ordering, porous or anisotropic constructs.

Zinc oxide is an important semiconductor in the chemical, agricultural, pharmaceutical, and personal care industries; such variety of applications is driven by its advantageous mechanical, thermal, optical and electronic properties [2,3]. Additionally, it is biocompatible and possesses useful bioactive properties [4,5]. All these properties are strongly influenced by its physical characteristics such as the micro-structure, particle size and crystallinity [6]. A wide range of physical,

chemical and biological methods are employed to produce zinc oxide [7]. Common preparation techniques include mechanochemical process [8–11], precipitation with and without surfactants present [12–16], (micro)emulsion techniques [17,18], sol-gel [19–21], solvothermal [22], hydrothermal [23–25], and microwave assisted methods [26,27]. Among these techniques, hydrothermal synthesis uses green solvent (water) and lower reaction temperatures, it typically involves one-step and is relatively straightforward process [28]. Moreover, hydrothermal methodology can incorporate control through temperature, reaction time and pH yielding various shapes: baton-, star-, flower- and rod-like ZnO crystals [29–32].

There are a few examples using polysaccharides in the fabrication of ZnO composites. For instance, Xu. C et al. reported the modification of the surface of ZnO particles synthesised by sol gel method with polysaccharides from fungal microorganisms [33]. Ma et al. synthesised ZnO-cellulose nanocomposites using a colloid mil and demonstrated that cellulose significantly affected the size and shape of the composites due to the formation of nano-network between many OH groups of cellulose and the surface of ZnO making ZnO immovable controlling agglomeration of ZnO [34]. Other examples include ZnO-starch

* Corresponding author at: School of Design, University of Leeds, Leeds LS2 9JT, UK.

E-mail address: n.sergeeva@leeds.ac.uk (N.N. Sergeeva).

<https://doi.org/10.1016/j.mtcomm.2023.107257>

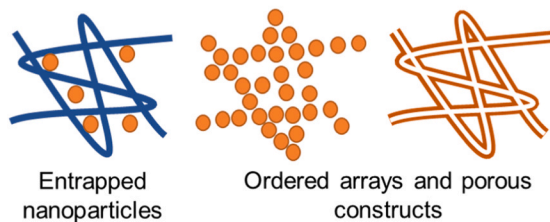
Received 17 July 2023; Received in revised form 13 September 2023; Accepted 5 October 2023

Available online 9 October 2023

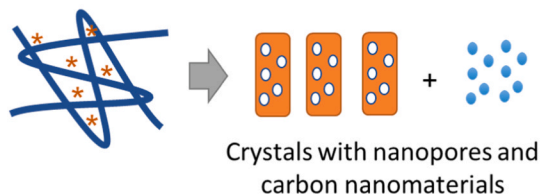
2352-4928/© 2023 The Authors. Published by Elsevier Ltd. This is an open access article under the CC BY license (<http://creativecommons.org/licenses/by/4.0/>).

composites synthesised by a precipitation method, ZnO-soybean polysaccharide film synthesised by casting method, [35,36] preparation of ZnO-chitosan by dispersion [37] and sol-gel conditions [38].

Previous work:



This work:



Previously published studies on the hydrothermal treatment of biopolymers or biomass focus mostly on the formation of carbonaceous sponges, carbon spheres and carbon dots through the degradation and carbonisation of macromolecules [39–41]. To the best of our knowledge, hydrothermal approach using chitosan as a template in ZnO synthesis has not been explored yet. We demonstrate that the use of rigid chitosan framework determines size (*nano* and *macro*), morphology and dimensionality (1D, 2D and 3D) of the ZnO composites, and the choice of the preparation strategy is a key. Our work shows how the biopolymer's thermal versatility can be exploited to form nanoporous crystals of ZnO, doped carbonaceous spheres as well as carbon dots. Furthermore, this study explores the role of chitosan and its effect on the optical, structural and antioxidant properties of the final materials.

2. Experimental section

2.1. Materials and methods

All chemicals were of analytical reagent grade and used without further purification. Chitosan (310–375 kDa, >75% deacetylation, coarse ground flakes and powder) was purchased from Aldrich. Zinc acetate dihydrate (97 + %) was purchased from Alfa Aesar. Sodium hydroxide, 35% ammonia solution and ammonia acetate were purchased from Fisher Chemical. Fluorescence data was recorded using Fluoromax spectrofluorometer. Fourier transform infrared (FT-IR) data was recorded using a PerkinElmer Spectrum One FT-IR spectrometer, with 300 scans, in the range of 550–4000 cm^{-1} . For powder x-ray diffraction (PXRD) analysis, approximately 20 mg of a sample was placed on the Si plate holder, and the diffraction data was collected on D2 PHASER BRUKER and Diffrac Commander Software using Cu X-ray source (CuK α wavelength of 1.5418 Å) and a range of 12–65°. Thermogravimetric analyser (TGA, SDT-Q600 Simultaneous TGA) was used to analyse the composition of the samples. The data obtained from FT-IR and PXRD were analysed using Origin. Scanning electron microscopy (SEM, FEI NOVA 450, coating unit 4 nm of iridium) was used to analyse the topography of the particle surface.

2.2. Focused ion beam (FIB)-SEM analysis and preparation of annealed samples

Cross sections through the crystals were prepared using FIB milling with a FEI Helio G4 CX dual-beam high-resolution monochromated FEG SEM instrument equipped with a FIB. A selected area of the crystal was

precoated with 2 μm thick Pt. The operating voltage was 30 kV, and the beam currents were varied between 0.1 and 5 nA. To prepare annealed samples for FIB-SEM, ZnO-CS composites synthesised at 180 °C and 220 °C were annealed at 700 °C for 3 h in the oven; the heating rate to reach the annealing temperature was set to 10 °C per min.

2.3. Synthesis of ZnO and ZnO composites

2.3.1. Synthesis of ZnO

To a 35% ammonia solution (2.5 mL) in deionised water (12.5 mL) NaOH (0.15 g, 3.64 mmol) was added followed by zinc acetate dihydrate (0.28 g, 1.25 mmol) under stirring. The mixture was continuously stirred and then set to reflux at a constant temperature of 60 °C for 1 h. The mixture was transferred to a Teflon-lined autoclave, sealed, and placed in the oven at 180 °C or 220 °C for 24 h hydrothermal treatment. The resulting mixture was centrifuged. The solid residue was separated from the supernatant, washed with deionised water, and centrifuged; this procedure was repeated three times. The white solid was dried in a vacuum oven at 60 °C.

2.3.2. Synthesis of ZnO-CS composites

Ammonia solution (2.5 mL, 35%) and deionised water (12.5 mL) were added to a 100 mL round bottom flask. Chitosan (0.28 g, 0.18 mmol) was added to the solution and sonicated at 30 °C for 5 min. NaOH (0.14 g, 3.61 mmol) was then added to the chitosan suspension with stirring and to this zinc acetate dihydrate (0.28 g, 1.27 mmol) was added. The solution was set to reflux at a constant temperature of 60 °C for 1 h with a continuous stirring. A pH of 12 was recorded before the mixture was transferred to a Teflon-lined autoclave, sealed, and placed in the oven at 180 °C or 220 °C for 24 h hydrothermal treatment. The supernatant (pH 10) resulting from the reaction mixture was collected. The solid washed 3 times with deionised water and once with ethanol and dried at 60 °C.

2.3.3. ZnO-ExCS composites

Ammonia solution (2.5 mL, 35%) and deionised water (12.5 mL) were added to a 100 mL round bottom flask. Chitosan (1.37 g, 0.90 mmol) was added to the solution and sonicated at 30 °C for 5 min. NaOH (0.14 g, 3.47 mmol) was then added to the chitosan suspension with stirring; after that zinc acetate dihydrate was added (0.27 g, 1.24 mmol). The solution was set to reflux at a constant temperature of 60 °C for 1 h with a continuous stirring. A pH of 12 was recorded before the mixture was transferred to a Teflon-lined autoclave, sealed, and placed in the oven at 180 °C or 220 °C for 24 h hydrothermal treatment. The supernatant (pH 10) resulting from the reaction mixture was collected. The solid washed 3 times with deionised water and once with ethanol and dried at 60 °C.

2.3.4. ExZnO-CS composites

Ammonia solution (2.5 mL, 35%) and deionised water (12.5 mL) were added to a 100 mL round bottom flask. Chitosan (0.28 g, 0.183 mmol) was added to the solution and sonicated at 30 °C for 5 min. NaOH (0.14 g, 3.60 mmol) was then added to the chitosan suspension with stirring and to this zinc acetate dihydrate was added (1.37 g, 6.26 mmol). The solution was set to reflux at a constant temperature of 60 °C for 1 h with a continuous stirring. A pH of 12 was recorded before the mixture was transferred to a Teflon-lined autoclave, sealed, and placed in the oven at 180 °C or 220 °C for 24 h hydrothermal treatment. The supernatant (pH 10) resulting from the reaction mixture was collected. The solid washed 3 times with deionised water and once with ethanol and dried at 60 °C.

2.4. Synthesis of CS carbon dots

Ammonia solution (2.5 mL, 35%) and deionised water (12.5 mL) were added to a 100 mL round bottom flask. Chitosan (0.28 g,

0.18 mmol) was added to the solution and sonicated at 30 °C for 5 min. NaOH (0.14 g, 3.61 mmol) was then added to the chitosan suspension with stirring and to this ammonium acetate dihydrate (0.1 g, 1.27 mmol) was added. The solution was set to reflux at a constant temperature of 60 °C for 1 h with a continuous stirring. A pH of 12 was recorded before the mixture was transferred to a Teflon-lined autoclave, sealed, and placed in the oven at 180 °C for 24 h hydrothermal treatment. The supernatant resulting from the reaction mixture was collected and centrifuged. The precipitate was separated from the solution, which contained dispersed carbon dots.

2.5. DPPH antioxidant activity assay

In brief, a 0.12 mM DPPH stock solution in ethanol and 10 mg/mL stock solutions of ZnO, CS and synthesised composites in DMSO were prepared. To prepare the range of the concentrations (0.04–0.4 mg/mL) in 96-well plate, the aliquots (0.001–0.01 mL) of the stock solution of an appropriate material were mixed with ethanol to make the final volume of 0.15 mL in each well (SI Fig. S4). To each well containing an appropriate concentration of the sample, 0.10 mL of DPPH stock solution was added and mixed well with a multichannel pipette (final volume in each well of 0.25 mL). The final concentrations of the composites were 0.04, 0.08, 0.12, 0.16, 0.2, 0.3 and 0.4 mg/mL. After incubating the plate for 30 min in the dark, the absorption spectra of the samples from each well were recorded. The A_0 and A_n values were measured as intensities of the absorption peak at 517 nm from the UV–vis spectrum of each sample after background subtraction. Radical scavenging activity (% RSA) was calculated using the equation: (% RSA) = $(A_0 - A_n) / A_0 \times 100\%$, where A_0 is the absorbance of DPPH solution and A_n is the absorbance of DPPH with the corresponding concentration of ZnO/CS material. The experiments were run in triplicates (SI Fig.S4).

3. Results and discussion

3.1. Synthesis

Zinc oxide and its composites with chitosan were prepared by hydrothermal method using a two-step procedure. Three different mass ratios of Zn-precursor (zinc acetate) and chitosan (CS) were tested to fabricate ExZnO-CS ($5_{Zn}:1_{CS}$), ZnO-CS ($1_{Zn}:1_{CS}$) and ZnO-ExCS ($1_{Zn}:5_{CS}$). Two reaction temperatures: 180 °C (@180) and 220 °C (@220) were selected for comparison. Initially, chitosan is pre-treated with ammonia solution at 30 °C under sonication for 5 min followed by the addition of zinc acetate dihydrate dissolved in aqueous solution of NaOH. The resulting mixture was heated at 60 °C for 1 h to facilitate deprotonation of CS and initiate ZnO formation. Finally, the hydrothermal treatment for 24 h at elevated temperature (180 °C and 220 °C) was performed to facilitate thermal decomposition of chitosan. After hydrothermal treatment, the reaction mixture was centrifuged to separate solid (composites) and supernatant (SUP). The supernatants are labelled as: SUP_ZnO-ExCS, SUP_ZnO-CS and SUP_ExZnO-CS corresponding to the following original loading ratios: $1_{Zn}:5_{CS}$, $1_{Zn}:1_{CS}$ and $5_{Zn}:1_{CS}$, respectively.

3.2. Analysis of composites

Obtained solid materials were primarily ZnO (Wurtzite, JCPDS 36–1451) [42] as confirmed by PXRD analysis (see SI Figs.S1a and 1b) showing the diffraction pattern of ZnO and all ZnO-CS composites synthesised at 180 °C and 220 °C. The peaks centred at 32.0°, 34.6°, 36.4°, 47.8°, 56.9° and 63.2° are attributed to (100), (002), (101), (102), (110) and (103), respectively. The PXRD pattern of pure untreated chitosan is characterised by two broad peaks centred at 9.5° (002), 20.2° (110) and a broad shoulder between 30° and 40°. The percent crystallinity of CS calculated by the PXRD integration method is 55% reflecting its partially amorphous nature. For the samples synthesised at 180 °C, the peaks at ca. 15.4° and 20.5° are recorded. This confirms that chitosan has

transformed into a new carbonaceous material by carbonisation process, which is consistent with the observation reported by Hammi et al. for carbonised chitosan [43]. Moreover, samples ZnO-CS@ 220 and ExZnO-CS@ 220 show only sharp diffraction pattern of wurtzite structure of ZnO indicating almost complete degradation of chitosan at 220 °C. The PXRD pattern of ZnO-ExCS@ 220 sample, however, features a broad band and a low intensity pattern of ZnO wurtzite (100), (002) and (101) with a percent crystallinity of 18% for this sample. The average crystallinity (based on ZnO pattern) decreases as the ratio of chitosan in the reaction increases for both temperatures revealing the formation of an amorphous material. The FT-IR analysis provides key evidence of the chitosan carbonisation (SI Figs.S1c and S1d); the features primarily affected are specific to the fingerprint region and include N-H (1584 cm^{-1}), CH-OH (1418 cm^{-1}), CH₂-OH (1375 cm^{-1}) and C-N (1371 cm^{-1}) stretches. It is clear that only ZnO-ExCS@ 180 sample displays features of dehydrated chitosan; but a significant broadening of the aforementioned typical CS stretches is observed in ZnO-CS@ 180 and ExZnO-CS@ 180 samples. While @ 180 series features chitosan as a part of the sample's composition, the FT-IR spectra for @ 220 series show drastic changes in the fingerprint region, which is very dissimilar to original chitosan. Two regions centred at 1562 cm^{-1} and 1376 cm^{-1} associated with acetylation degree have been gradually replaced by a broad less defined band. Furthermore, the retention of 2928 cm^{-1} signal assigned to asymmetric C-H stretch is observed supporting carbonisation of chitosan.

TGA analysis of the composites is summarised in Fig. 1, where the total % weight loss was calculated at 700 °C as no further decomposition was observed beyond this temperature. The total weight loss of pure ZnO is only 0.6%, which is attributed to the loss of moisture. The degradation range of chitosan occurred between 200 °C and 650 °C, which is perfectly consistent with the literature [44]. Overall, ZnO content for the series synthesised at 220 °C is larger compared to the series synthesised at 180 °C. The first derivative analysis (Fig. 1b and d) reveals three distinct regions in the decomposition of chitosan with the inflection temperatures (T_i) of 279 °C, 479 °C and 597 °C with a rapid first stage. The first step is attributed to the degradation of chitosan, while the second step relates to the carbonisation process [45,46]. The @ 180 series follow similar thermal decomposition behaviour for pure chitosan with a slight shift of the first T_i and lacking defined third stage. The thermal decomposition pattern for @ 220 series is very different and shows no real similarities with original chitosan. Here, the decomposition happens at higher temperature and mostly finishes at 600 °C.

3.3. SEM analysis

Based on SEM analysis, all ZnO-CS composites, except ZnO-ExCS@ 220, exhibit common rod-like morphology (SI Fig.S2) [29]. The average length of the rods varies between 2.7 μm and 7.3 μm (analysis by ImageJ). As excess of Zn precursor increases the crystal size (both width and length) increases too indicating the growth, while the rods of a smaller diameter are observed with excess of CS; here, chitosan may inhibit growth of ZnO and lead to crystals of a smaller diameter. Also, the crystals appear to be 'coated' supporting the existence of composite material rather than physical mixture of CS and ZnO. In contrast, SEM images of ZnO-ExCS@ 220 show homogeneous spherical morphology with a particle size of 37–80 nm; this observation is supported by PXRD indicating its mostly amorphous nature. This domination of 1D morphology is likely driven by efficient carbonisation of the biopolymer resulting in the formation of carbonaceous spheres doped with ZnO.

The samples were subjected to FIB procedure to further understand structural features of ZnO-CS composites. Cuts across the samples reveal pores. Fig. 2b shows a cross-section (transverse) cut of the ZnO-CS@ 180 crystals where the pore size ranges from 7 nm to 42 nm. Longitudinal cut through ZnO-CS@ 220 reveals the pore size between 8 nm and 76 nm (Fig. 2d). To better understand the origin of pores and their content, annealing experiments of ZnO-CS samples synthesised at

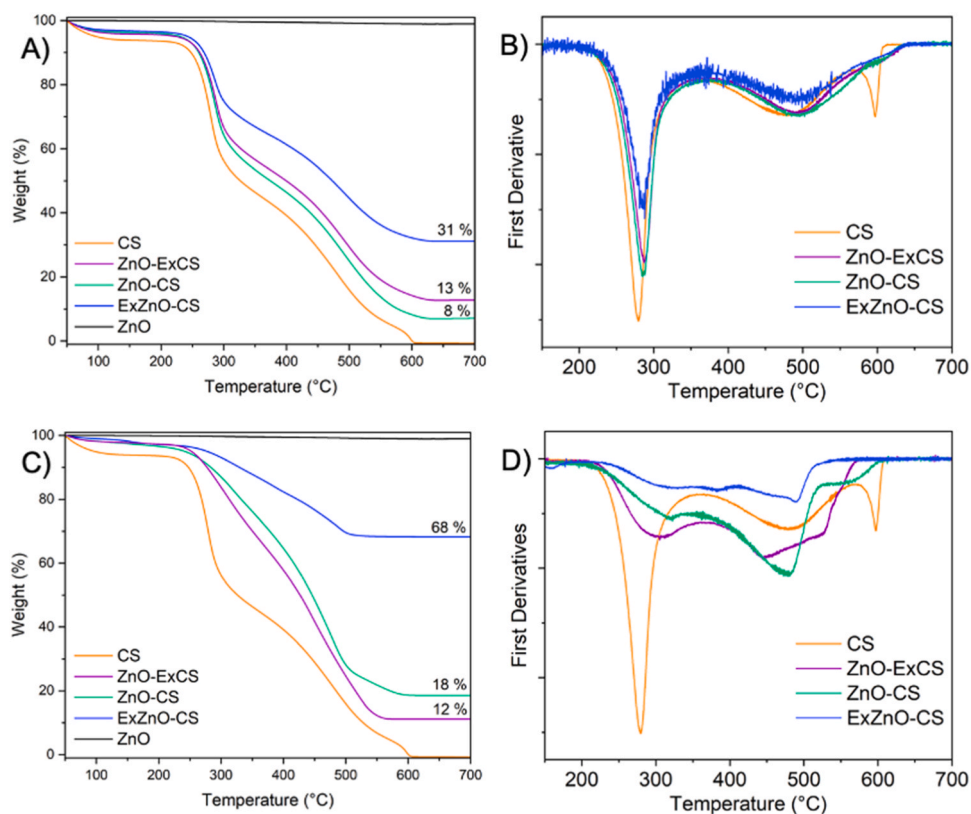


Fig. 1. TGA data with the percentages of the remaining ZnO at 700 °C: (a) TGA data for @ 180 series; (b) 1st derivative for @ 180 series; (c) TGA data for @ 220 series; (d) 1st derivative for @ 220 series.

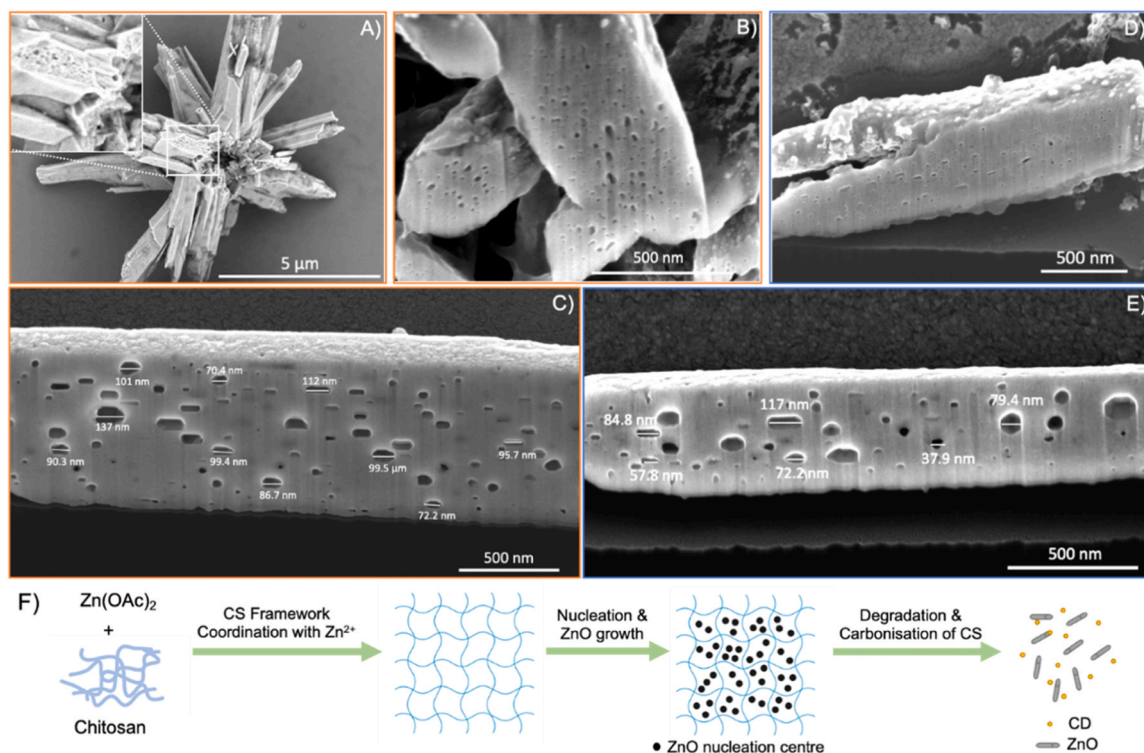


Fig. 2. (a) SEM image of original ZnO-CS synthesised at 180 °C; (b) FIB-SEM images of original ZnO-CS synthesised at 180 °C and (c) annealed ZnO-CS synthesised at 180 °C; (d) FIB-SEM image of original ZnO-CS synthesised at 220 °C and (e) FIB-SEM image of annealed ZnO-CS synthesised at 220 °C. (f) Schematic diagram of ZnO potential growth within chitosan framework.

180 °C and 220 °C have been carried out. The annealing temperature of 700 °C was selected based on the TGA data indicating complete degradation of any organic residual by 650 °C. SEM images of the annealed ZnO-CS composites are shown in Fig. 2c and e.

After annealing, the pore size observed in the longitudinal cuts for both ZnO-CS@ 180 and ZnO-CS@ 220 is similar and ranges from 8 nm to 137 nm suggesting a universal mechanism of co-growth. The maximum pore size for ZnO-CS@ 180 has increased significantly to 137 nm after annealing. This data demonstrates that during the co-growth of ZnO with CS, the pores are formed within ZnO matrix. They are partially filled with CS residuals and therefore appear smaller in “not-annealed” SEM images. After annealing these residuals are destroyed revealing the true size of pores within ZnO matrix.

Schematics of how ZnO can grow within biopolymer framework is shown in Fig. 2f. In short, the chitosan framework serves as a template to coordinate Zn^{2+} ions through -OH and -NH₂ groups of CS. This entraps Zn^{2+} ions making them immobile and integrating the centres of nucleation within the template. This is followed by the aggregation of insoluble Zn(OH)₂ and subsequent ZnO growth entrapping chitosan within. An elevated temperature during the hydrothermal treatment leads to the degradation of CS network leaving pores, which can still contain carbonised chitosan.

3.4. Fate of chitosan template

To further explore the role of chitosan, we have analysed supernatants (SUPs) from the corresponding hydrothermal reactions. All SUPs independent from the reaction conditions, showed a strong blue fluorescence (Fig. 3), which cannot originate from non-fluorescent chitosan. Moreover, the fluorescence maximum was ‘floating’ depending on the excitation energy, such behaviour is typical for carbon dots (CDs) due to the quantum confinement effect, varying size and surface traps

(functional groups) [47,48]. As CDs can be produced using top-down approach [48,49] by subjecting large molecules and polymers such as chitosan to pyrolysis, it is possible that chitosan, ammonia and acetate were involved in the generation of the suspected CDs in the SUPs rather than stopping at the stage of carbonaceous spheres.

To prove this, chitosan was hydrothermally treated using the same procedure only replacing Zn(OAc)₂ with ammonium acetate at 180 °C/ 220 °C for 24 h. Analysis of a liquid phase (light brown solution) and a solid residual from this reaction reveals that only the liquid phase (CS-CDs) was highly fluorescent; the emission spectra were collected at several excitation wavelengths from 300 nm to 400 nm with 10 nm increments (Fig. 3a). A red shift of the emission band from 395 nm to 465 nm for both reaction temperatures is evident as the excitation wavelength increases confirming the wavelength of the emission maximum being dependent on the excitation energy (Fig. 3a and b).

There are some parallels between the emission spectra of chitosan CDs (CS-CDs) and the SUPs obtained from the preparation of ZnO composites (Fig. 3c and d). The SUPs emit in the same region (395–465 nm), which suggests a similar CD composition. Although CS-CDs prepared at 220 °C emit at 466 nm when excited at 390 nm, the behaviour of individual SUPs in @ 220 series closely resembles the SUP@ 180 series (Fig. 3d). Some broadening of the emission peak is observed for SUP@ 220 series suggesting CDs with a varied particle size. This is expected as the higher temperature of the reaction facilitates the carbonisation of chitosan leading to variation in the particle size of newly formed carbon dots.

Additionally, the UV–vis spectra of the SUPs obtained at 180 °C and 220 °C are similar showing a featureless broad band with a shoulder centred at ca. 260–268 nm. This aligns well with the UV absorption profiles of CS-CDs synthesised at 180 °C and 220 °C. The absorption above 260 nm can be attributed to the $\pi \rightarrow \pi^*$ and $n \rightarrow \pi^*$ electronic transitions in the newly created CDs [50].

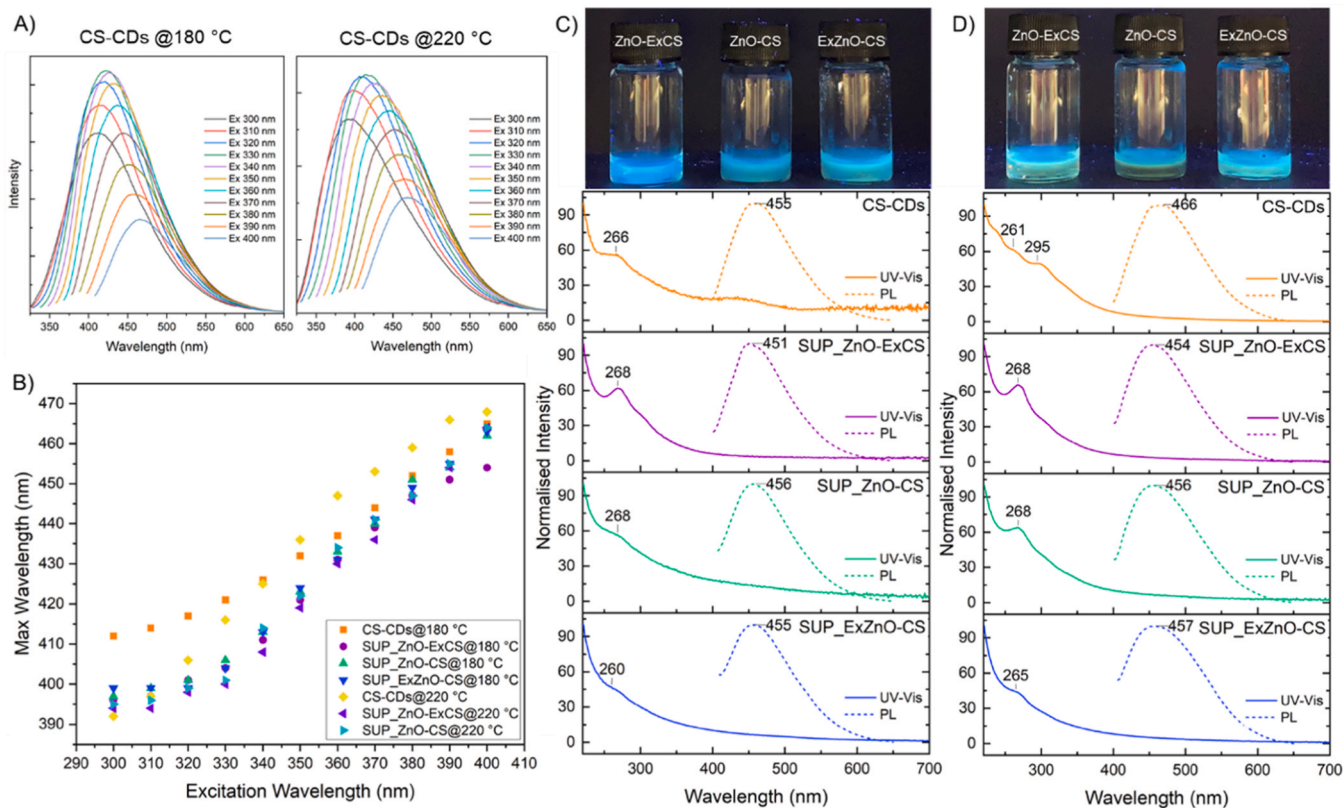


Fig. 3. (a) “Floating” PL of CS-CDs. (b) PL wavelength at λ_{max} measured in fluorescence for CS-CDs and SUPs. UV–vis and PL spectra (excited at 390 nm) of the SUP synthesised: (c) at 180 °C and (d) at 220 °C, with pictures taken under the standard UV lamp at 365 nm.

The presence of carbon dots should also be detectable in the composites; thus, the ZnO-CS solid materials were dispersed in water and the emission spectra were recorded at the excitation wavelength range of 300–400 nm. All ZnO-CS composites exhibit photoluminescence between 450 and 470 nm; in contrast, pure ZnO does not emit in this region (see SI Fig.S3). This also strongly supports that carbonised CS is detained by ZnO matrix.

Finally, FTIR analysis of dried SUPs and only chitosan-CDs is summarised in Fig. 4a and b. Although the C-H stretch is a prominent peak in chitosan and composites, in all the SUPs, including CS-CDs, the C-H stretch (2928 cm^{-1}) is a much less significant peak. This coupled with the loss of intensity of the C-H bending vibrations ($1165\text{--}992\text{ cm}^{-1}$) suggests degradation of the chitosan chain and pyranose ring, through dehydration. Additionally, it is evident that the N-H peak ($1550\text{--}1590\text{ cm}^{-1}$) is prominent in all SUPs. Overall, this is consistent with what has been found for amino-functionalised fluorescent carbon nanoparticles in the literature [40].

3.5. Evaluation of antioxidants activity

A suspended benefit of CS-incorporated ZnO is additional antioxidant activity. The antioxidant capabilities were determined by DPPH radical scavenging spectrophotometric assay. 1,1-Diphenyl-2-picrylhydrazyl (DPP $^{\cdot}$) is a stable free radical with a visible absorption maximum at 517 nm. It is often used as an equivalent of OH radical to assess an antioxidant's efficiency. We have employed our previously reported DPPH protocol for the analysis of heterogeneous samples [51] within the attainable accuracy range to minimise experimental errors corresponding to the transmittance window of 20–60% [52] for spectrophotometric measurements. In this study, the final DPPH concentration was 0.048 mM, and the concentration range of ZnO, CS and the composites was 0.04–0.4 mg/mL. The radical scavenging reaction was started by the addition of 0.1 mL of DPPH stock solution to the prepared solutions containing the composites (0.15 mL). The A_0 and A_n values have been measured as intensities of the absorption peak at 517 nm from the control and the samples. The antioxidant activity of ZnO, CS and the composites is summarised in Fig. 4c and d. Pure ZnO is an inefficient

radical scavenger at low concentrations (11%, 0.04 mg/mL), although % antioxidant activity improves up to 40% at higher concentrations. The composites synthesised at $180\text{ }^{\circ}\text{C}$ show a moderate antioxidant activity with ExZnO-CS exhibiting the highest efficiency (54%), followed by ZnO-CS (33%) and ZnO-ExCS (28%) with the latter two featuring below ZnO itself. Such behaviour could be explained by the presence of the residual CS in the composites, which potentially inhibits radical scavenging activity of the materials. In contrast, the composites prepared at $220\text{ }^{\circ}\text{C}$ possess excellent antioxidant properties both at low and high concentrations. All samples can reach 100% of antioxidant activity at higher concentration. Moreover, ZnO-ExCS exhibit remarkably high activity even at very low concentrations (100% at 0.08 mg/mL), while ExZnO-CS reaches $> 90\%$ at the concentrations above 0.12 mg/mL. These results indicate that the carbonisation of CS into smaller entities such CDs can improve overall antioxidant activity of the composites. Antioxidant properties of CDs were previously reported [53,54]. It can also be added that ZnO-ExCS has a significantly smaller particle size and therefore, potentially a larger active surface area to deactivate the radicals. On the other hand, ExZnO-CS sample has the largest ZnO content (TGA, 68%) together with carbonised CS, which results in higher concentration of CDs in the composite as opposed to @ 180 series. It can be concluded that the presence of CDs may be a determining factor of antioxidant activity enhancement.

4. Conclusions

In conclusion, ZnO-CS composites were synthesised at two temperatures ($180\text{ }^{\circ}\text{C}$ and $220\text{ }^{\circ}\text{C}$) using a hydrothermal procedure. All materials were characterised by PXRD, FT-IR, TGA, SEM, FIB, UV-vis absorption and fluorescence spectroscopy. All materials in @ 180 series showed the wurtzite structure of ZnO along with new peaks originated from partial degradation of CS. In ExZnO-CS and ZnO-CS synthesised at $220\text{ }^{\circ}\text{C}$, characteristic pattern of the wurtzite ZnO is dominant, and a minor broad peak can be observed. However, this broad peak, which originates from carbonised CS, is prevalent in ZnO-ExCS accompanied by a low intensity pattern of ZnO. TGA analysis shows that the composites synthesised at $180\text{ }^{\circ}\text{C}$ contain residual CS. The analysis of the

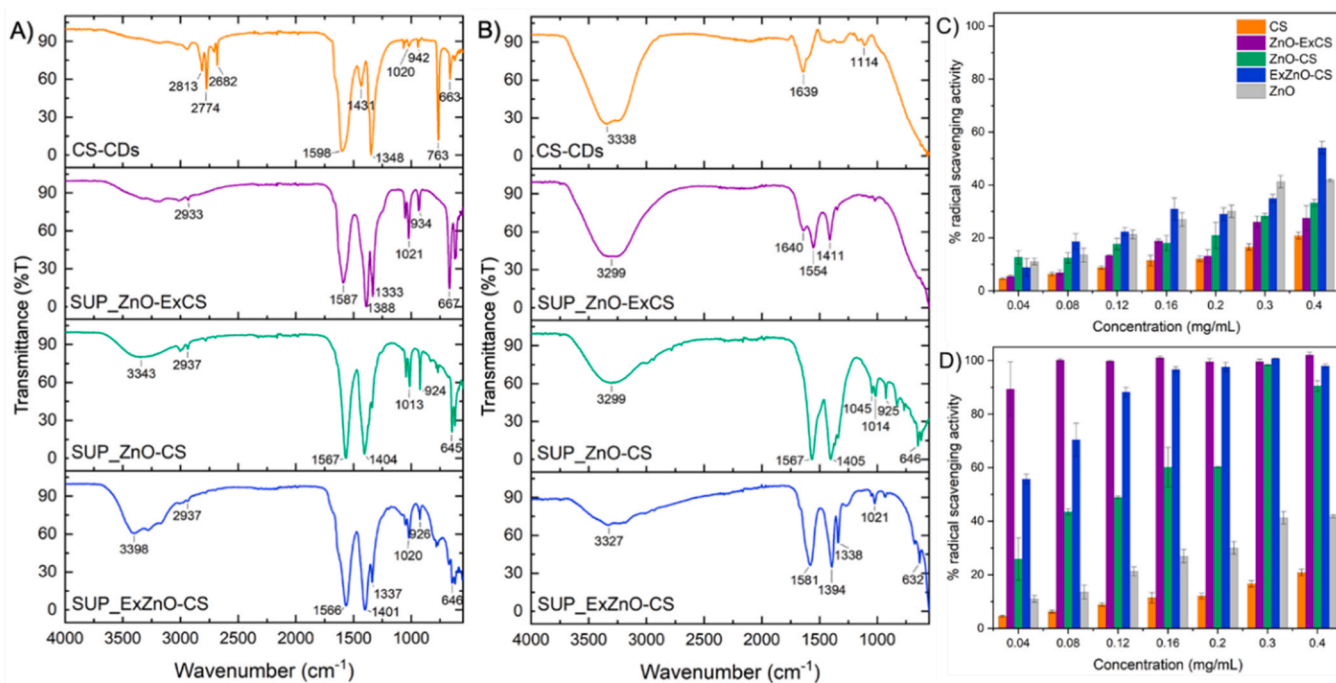


Fig. 4. FT-IR analysis of SUPs synthesised: (a) at $180\text{ }^{\circ}\text{C}$ and (b) at $220\text{ }^{\circ}\text{C}$. Radical scavenging activity measured by DPPH assay of ZnO, CS and composites: (c) synthesised at $180\text{ }^{\circ}\text{C}$ and (d) synthesised at $220\text{ }^{\circ}\text{C}$.

first derivative plots for both series shows a drastic difference. The thermal decomposition pattern for @ 220 series does no longer resemble the original CS. Also, ZnO content for the composites synthesised at 220 °C was larger as CS degraded faster at higher temperature. The SEM analysis reveals the shape, size, and the presence of pores in the materials. Additional experiments point out that the CS carbonisation during the synthesis leads to the formation of pores and as a by-product the carbon dots are produced. The formation of CDs was probed by fluorescence spectroscopy revealing the floating like behaviour of the emission maxima. Also, FT-IR analysis provided key evidence of the CS carbonisation in the composites. Finally, the antioxidant activity of the materials was determined by DPPH assay. The composites synthesised at 180 °C showed moderate radical scavenging activity, while those synthesised at 220 °C exhibited excellent activity in comparison to pure ZnO.

CRedit authorship contribution statement

NNS conceived the project and KK led all the experiments and characterization with assistance of SC, GM and AK. The manuscript was written through contributions of all authors. All authors have given approval to the final version of the manuscript.

Declaration of Competing Interest

The authors declare the following financial interests/personal relationships which may be considered as potential competing interests. Kanako Kimura reports financial support was provided by Japan Student Services Organization.

Data Availability

No data was used for the research described in the article.

Acknowledgements

This work was supported through the Watanabe Foundation, Japan Student Services Organization (JASSO), the Leeds Institute of Textiles and Colour (LITAC) and the University of Leeds.

Appendix A. Supporting information

Supplementary data associated with this article can be found in the online version at [doi:10.1016/j.mtcomm.2023.107257](https://doi.org/10.1016/j.mtcomm.2023.107257).

References

- [1] Z. Schnepf, *Angew. Chem. Int. Ed.* 52 (2013) 1096–1108.
- [2] E. Bacaksiz, M. Parlak, M. Tomakin, A. Özçelik, M. Karakız, M. Altunbaş, *J. Alloy. Compd.* 466 (2008) 447–450.
- [3] Y. Zhang, M.K. Ram, E.K. Stefanakos, D.Y. Goswami, *J. Nanomater.* 2012 (2012), e624520.
- [4] J. Jiang, J. Pi, J. Cai, *Bioinorg. Chem. Appl.* 2018 (2018) 1–18.
- [5] S. S.S, H. Kumari, R. Kandasamy, S. Muthusamy, *Materials Science and Engineering C*, DOI: (10.1016/j.msec.2017.05.059).
- [6] O.P. Egambaram, S. Kesavan Pillai, S.S. Ray, *Photochem. Photobiol.* 96 (2020) 779–797.
- [7] A. Kotodziejczak-Radzimska, T. Jesionowski, *Materials* 7 (2014) 2833–2881.
- [8] W. Ao, J. Li, H. Yang, X. Zeng, X. Ma, *Powder Technol.* 168 (2006) 148–151.
- [9] A. Stanković, Lj Veselinović, S.D. Skapin, S. Marković, D. Uskoković, *J. Mater. Sci.* 46 (2011) 3716–3724.
- [10] T. Tsuzuki and P. McCormick, *Scripta Materialia*, DOI: (10.1016/S1359-6462(01)00793-X).
- [11] A. Moballeghe, H.R. Shahverdi, R. Aghababazadeh, A.R. Mirhabibi, *Surf. Sci.* 601 (2007) 2850–2854.
- [12] A. Kotodziejczak-Radzimska, T. Jesionowski, A. Krysztafkiwicz, *Physicochem. Probl. Miner. Process.* 44 (2010) 93–102.
- [13] R. Hong, T. Pan, J. Qian, H. Li, *Chem. Eng. J.* 119 (2006) 71–81.
- [14] Z. Cao, Z. Zhang, F. Wang, G. Wang, *Colloids Surf. A Physicochem. Eng. Asp.* 340 (2009) 161–167.
- [15] P. Li, Y. Wei, H. Liu, X. Wang, *J. Solid State Chem.* 178 (2005) 855–860.
- [16] Y. Wang, C. Ma, X. Sun, H. Li, *Inorg. Chem. Commun.* 5 (2002) 751–755.
- [17] C.-H. Lu, C.-H. Yeh, *Mater. Lett.* 33 (1997) 129–132.
- [18] X. Li, G. He, G. Xiao, H. Liu, M. Wang, *J. Colloid Interface Sci.* 333 (2009) 465–473.
- [19] T.H. Mahato, G.K. Prasad, B. Singh, J. Acharya, A.R. Srivastava, R. Vijayaraghavan, *J. Hazard. Mater.* 165 (2009) 928–932.
- [20] H. Benhebal, M. Chaib, T. Salmon, J. Geens, A. Léonard, S. Lambert, M. Crine, B. Heinrichs, *Alex. Eng. J.* 52 (2013) 517–523.
- [21] M. Ristić, S. Musić, M. Ivanda, S. Popović, *J. Alloy. Compd.* 397 (2005) L1–L4.
- [22] S.-J. Chen, L.-H. Li, X.-T. Chen, Z. Xue, J.-M. Hong, X.-Z. You, *J. Cryst. Growth* 252 (2003) 184–189.
- [23] D. Chen, X. Jiao, G. Cheng, *Solid State Commun.* 113 (1999) 363–366.
- [24] A.A. Ismail, A. El-Midany, E.A. Abdel-Aal, H. El-Shall, *Mater. Lett.* 59 (2005) 1924–1928.
- [25] L.N. Dem'yanets, L.E. Li, T.G. Uvarova, *J. Mater. Sci.* 41 (2006) 1439–1444.
- [26] J. Jörg, R.C. Schneider, J. Hoffmann, A. Engstler, E. Klyszcz, P. Erdem, R.-A. Jakes, L. Eichel, Pitta-Bauerermann, J. Bill, *Chem. Mater.* 22 (2010) 2203–2212.
- [27] L. Schmidt-Mende, J.L. MacManus-Driscoll, *Mater. Today* 10 (2007) 40–48.
- [28] Ş.Ş. Türkyılmaz, N. Güy, M. Özacar, J. Photochem. Photobiol. A Chem. 341 (2017) 39–50.
- [29] A.R. Marlinda, N. Yusoff, A. Pandikumar, N.M. Huang, O. Akbarzadeh, S. Sagadevan, Y.A. Wahab, M.R. Johan, *Int. J. Hydrog. Energy* 44 (2019) 17535–17543.
- [30] S. Baruah, J. Dutta, *Sci. Technol. Adv. Mater.* 10 (2009), 013001.
- [31] K. Edalati, A. Shakiba, J. Vahdati-Khaki, S.M. Zebarjad, *Mater. Res. Bull.* 74 (2016) 374–379.
- [32] M. Ramya, T.K. Nideep, V.P.N. Nampoori, M. Kailasnath, *Sci. Rep.* 11 (2021) 6159.
- [33] C. Xu, M. Ojeda, R.A.D. Arancón, A.A. Romero, J.L. Domingo, M. Gómez, J. Blanco, R. Luque, *ACS Sustain. Chem. Eng.* 3 (2015) 2716–2725.
- [34] J. Ma, Z. Sun, Z. Wang, X. Zhou, *Cellulose* 23 (2016) 3703–3715.
- [35] B. Jurca, A. Tirsoaga, A. Ianculescu, O. Carp, *J. Therm. Anal. Calor.* 115 (2014) 495–501.
- [36] M. Akbariazam, M. Ahmadi, N. Javadian, A. Mohammadi Nafchi, *Int. J. Biol. Macromol.* 89 (2016) 369–375.
- [37] O.S. Kushwaha, C.V. Avadhani, R.P. Singh, *Carbohydr. Polym.* 123 (2015) 164–173.
- [38] I. Ben Amor, H. Hemmami, S.E. Laouini, M.S. Mahboub, A. Barhoum, *Catalysts* 12 (2022) 1611.
- [39] S. Yu, X. Dong, P. Zhao, Z. Luo, Z. Sun, X. Yang, Q. Li, L. Wang, Y. Zhang, H. Zhou, *Nat. Commun.* 13 (2022) 3616.
- [40] Y. Yang, J. Cui, M. Zheng, C. Hu, S. Tan, Y. Xiao, Q. Yang, Y. Liu, *Chem. Commun.* 48 (2012) 380–382.
- [41] B. Hu, K. Wang, L. Wu, S.-H. Yu, M. Antonietti, M.-M. Titirici, *Adv. Mater.* 22 (2010) 813–828.
- [42] M. Guo, P. Diao, S. Cai, *J. Solid State Chem.* 178 (2005) 1864–1873.
- [43] N. Hammi, N. Marcotte, M. Marinova, K. Draoui, S. Royer, A. El Kadib, *Carbohydr. Polym. Technol. Appl.* 2 (2021), 100043.
- [44] M.A. Diab, A.Z. El-Sonbati, M.M. Al-Halawany, D.M.D. Bader, *Open J. Polym. Chem.* 2 (2012) 14–20.
- [45] V.M. Muinde, J.M. Onyari, B. Wamalwa, J.N. Wabomba, *Environ. Chem. Ecotoxicol.* 2 (2020) 115–125.
- [46] M. Ahmed, H. Youssef, S.M. Abou-Yousef, El-Sayed, S. Kamel, *Int. J. Biol. Macromol.* 76 (2015) 25–32.
- [47] L. Sun, H. Zhang, Y. Wang, Z. Xiong, X. Zhao, Y. Xia, *Spectrochim. Acta Part A Mol. Biomol. Spectrosc.* 251 (2021), 119468.
- [48] M.L. Liu, B.B. Chen, C.M. Li, C.Z. Huang, *Green. Chem.* 21 (2019) 449–471.
- [49] H. Li, Z. Kang, Y. Liu, S.-T. Lee, *J. Mater. Chem.* 22 (2012) 24230.
- [50] N. Hammi, N. Marcotte, M. Marinova, K. Draoui, S. Royer, A. El Kadib, *Carbohydr. Polym. Technol. Appl.* 2 (2021), 100043.
- [51] H. Yu, Z. Guo, S. Wang, G.S.N. Fernando, S. Channa, A. Kazlauciusas, D.P. Martin, S.A. Krasnikov, A. Kulak, C. Boesch, N.N. Sergeeva, *ACS Biomater. Sci. Eng.* 5 (2019) 2778–2785.
- [52] G.H. Ayres, *Anal. Chem.* 21 (1949) 652–657.
- [53] M.H. Son, S.W. Park, Y.K. Jung, *Nanotechnology* 32 (2021), 415102.
- [54] Z. Ji, A. Sheardy, Z. Zeng, W. Zhang, H. Chevva, K. Allado, Z. Yin, J. Wei, *Molecules* 24 (2019) 152.